Stereology-Based Quantitative Characterization of Dispersion from TEM Micrographs of Polymer–Clay Nanocomposites

Soumendra K. Basu,[1] Paula D. Fasulo,[2] William R. Rodgers[2]

[1]*India Science Laboratory, General Motors R&D, Creator, ITPL, Bangalore 560066, India*
[2]*Materials and Processes Laboratory, General Motors R&D, Warren, Michigan 48090*

Received 9 October 2009; accepted 12 April 2010
DOI 10.1002/app.32756
Published online 27 July 2010 in Wiley Online Library (wileyonlinelibrary.com).

ABSTRACT: Quantitative characterization of the state of dispersion and extent of exfoliation is critical in developing processing structure–property relationships in polymer–clay nanocomposites. Quantification of dispersion, exfoliation, and nanostructure in polymer–clay nanocomposites by 3D stereological parameters using image analysis of 2D transmission electron microscopy (TEM) micrographs were recently proposed. The 3D dispersion quantifying parameters are designed such that they are free of the bias associated with not sampling the true particle diameter in a 2D TEM section. In this article, the ability of the proposed 3D dispersion quantifying parameters to describe the dispersion over the entire possible range of exfoliation, and to capture independent aspects of dispersion are demonstrated by quantifying several sets of samples that were designed using a polypropylene (PP)/maleated PP/clay system. The details of the image analysis procedure, the underlying challenges, and errors involved in the segmentation process are also discussed. The 3D dispersion quantifying parameters, exfoliation number and inter-particle distance, were critically compared against the standard 2D dispersion quantifying parameters, such as mean length, thickness, and aspect ratio. In all cases examined in this study, the sensitivity and resolution of the 3D parameters in terms of quantifying the dispersion of the nanostructure appeared comparable if not better than the standard 2D parameters. © 2010 Wiley Periodicals, Inc. J Appl Polym Sci 119: 396–411, 2011

Key words: dispersions; exfoliation; clay; nanocomposites; microstructure

INTRODUCTION

Polymer–clay nanocomposites exhibit significantly improved mechanical, thermal, and barrier properties at fractional filler loadings compared with traditional composites prepared using micron(or larger)-size-fillers.[1,2] Better properties at lower weight, along with superior surface finish due to the nano-size of the clay fillers, make nanocomposites attractive for automotive exterior and interior trims, body panels, and a few underbody applications. For these non-structural automotive applications of polymer–clay nanocomposites, stiffness and appearance are of utmost importance, whereas the strength of the nanocomposite is of greater importance in semi-structural applications. The stiffness, strength, appearance, and other properties of a nanocomposite are dependent on the nano-size, volume fraction, degree of dispersion/exfoliation, and nanostructure of the clay fillers.[3–5] To attain the best possible properties, at economically affordable clay loadings, the dispersion, exfoliation, and nanostructure of the clay fillers need to be optimized. The state of dispersion and the nanostructure of the clay fillers can vary from fully exfoliated to intercalated to unexfoliated micro-composites to the more often observed combination of two or more of these morphologies. Detailed quantitative characterization of the state of dispersion and extent of exfoliation of the clay fillers is, therefore, of utmost importance, on the one hand, to design optimized nanostructures for the best properties, and on the other hand, to arrive at the best compositions and processing conditions required for obtaining the optimized nanostructure.

X-ray diffraction (XRD),[5–10] transmission electron microscopy (TEM),[5–17] rheology,[18–21] small angle X-ray scattering (SAXS),[8,22] wide angle X-ray diffraction (WAXD),[14] infrared spectroscopy,[23] permeability measurement,[24,25] and nuclear magnetic resonance (NMR)[26] have been used to characterize the state of dispersion and nanostructure in polymer–clay nanocomposites. XRD is useful in characterizing intercalated and unexfoliated macro-composites, where ordered, structures of the clay layers are preserved.

Correspondence to: S. K. Basu (soumendra.basu@gmail.com).

However, it is not so useful in randomly dispersed, disordered exfoliated samples where the intensity and sharpness of the XRD peaks are reduced with increasing extent of exfoliation. Measurements of complex viscosity and dynamic storage modulus at low-shear rates have also been extensively used to characterize clay dispersion.[18–20] All these techniques provide indirect, partial information about the state of exfoliation, and almost always are complemented with analysis of TEM micrographs of the samples, which is the only technique that provides direct information about the state of exfoliation and dispersion.

TEM micrographs are typically used to qualitatively describe whether a specimen is intercalated, exfoliated, or has a mixed morphology, and to qualitatively compare the morphologies of different samples. Several researchers have extended the qualitative assessment to quantitative analysis with various degrees of complexity ranging from manual particle counting to elaborate image analysis based measurements. Dennis et al.[7] counted the number of platelets or intercalates in a given area of the TEM micrograph and concluded that higher particle density indicates higher dispersion. Nam et al.[8] measured the average length, average thickness, and average inter-particle distance for specimens with different extents of clay loading. Paul and coworkers,[7,9–12] Marchant and Jayaraman,[6] and Ratinac et al.[14] used image analysis on TEM micrographs to quantify dispersion, and proposed particle length, thickness, aspect ratio, particle number density, distribution of the number of clay platelets per particle, exfoliation factor, etc. as quantitative measures of clay dispersion. Vermogen et al.[13] and Eckel et al.[5] measured inter-particle distances in the direction parallel and perpendicular to the mean particle orientation and linear inter-particle intercept distance, respectively. Kim et al.[15] applied statistical quantifiers/techniques such as Morisita index and skewness-quadrat method on TEM particle measurements to rank the samples and compared the results with visual observation. Although several quantifiers capturing different aspects of dispersion have been proposed in the literature, their ability to quantify the true 3D dispersion of a sample is limited because the quantifiers are measured directly from 2D TEM micrographs.

It is well known that measurements of direct and indirect dispersion quantifying parameters from 2D TEM micrographs, as stated in the above research, provide a biased characterization of the true 3D nanostructure.[11,16] This is because intrinsically the clay particles have various sizes and shapes, and, therefore, the size and the orientation of the platelets present at the TEM cross section and position of the cross sectional plane itself influences the measurement obtained from the 2D TEM micrographs.[11,16] Some of these limitations can be overcome by analysis of the 2D TEM micrographs using the science of stereology, wherein 2D stereological parameters are measured from the micrographs which are subsequently used to calculate 3D dispersion quantifying parameters using exact stereological equations.[16,17] Stereology is a well-evaluated science based on integral geometry and spatial statistics,[27–29] which relates the information of higher dimensions to that observed in lower dimension sections. As explained later, unlike directly measuring 2D length, thickness, and aspect ratio distributions as in the traditional approach; the proposed approach measures those 2D quantities from the segmented TEM micrographs which have exact stereological relationships with 3D microstructural attributes, and thereby eliminates the bias present in the traditional 2D measurements. Two parameters, the exfoliation number quantifying the extent of exfoliation and the inter-particle distance quantifying the mean separation between the clay particles, were recently proposed as two possible 3D quantifiers of the dispersion of clay particles in polymer–clay nanocomposites.[16] Although these proposed dispersion quantifying parameters by design are independent of the bias present in a 2D measurement, it is unknown how these parameters compare against traditional 2D parameters in capturing independent aspects of nanocomposite dispersion in samples having a wide range in exfoliation. This article, therefore, evaluates how well the proposed 3D parameters compare against traditional 2D parameters such as the mean length, the thickness, and the aspect ratio of the clay particles in terms of resolution, sensitivity, range, consistency, and ability to bring out hidden aspects of dispersion. In addition, the details of the image segmentation/analysis procedure, the challenges, and the errors involved in the segmentation process are also presented. The proposed 3D parameters are compared to the traditional 2D parameters by characterizing and quantifying the dispersion in samples with various types of nanostructure prepared using a polypropylene (PP)/maleated PP/clay system. Based on a critical evaluation of the proposed and traditional TEM-based nanostructure quantifying parameters, the advantages and the limitations of each of the parameters are evaluated.

EXPERIMENTAL

Materials

Four sets of nanocomposite formulations were designed for this study. The materials used and their sources are shown in Table I. Cloisite® 20A was the montmorillonite clay that was used as the

TABLE I
Materials, Their Commercial Names, and Suppliers

Supplier	Product name	Description
Lyondell Basell	HA1152	Homopolymer
Lyondell Basell	CA138A	Impact modifier
Lyondell Basell	CA207A	Impact modifier
Lyondell Basell	KC130	Copolymer
Lyondell Basell	PXH00A	Homopolymer
Lyondell Basell	PH020	Homopolymer
Chemtura	Polybond® 3200	Maleated polypropylene
The Dow Chemical Co.	Engage 8150	Elastomer
Southern Clay	Cloisite 20A	Organo-silicate filler
Southern Clay	Masterbatch 70 (MB 70)	Organo-silicate masterbatch
Ciba Specialty Chemicals	FS 210 FF	Antioxidant

reinforcing filler in these formulations and was either added directly or added as part of a masterbatch (masterbatch 70) which was composed of clay, maleated PP (PP-*g*-MA), and PP. The masterbatch had less than a 1 : 1 ratio of PP-*g*-MA/clay with the concentration of PP-*g*-MA lower than the clay. Wherever clay is added as part of the masterbatch, the clay wt % and PP-*g*-MA/clay ratio in the final formulation are presented in the composition tables for the relevant sets. A brief description of each set follows:

Set 1

This set of formulations was prepared to examine the ability of the proposed parameters to capture dispersion in samples covering a broad range of exfoliation. For these samples, the PP to PP-*g*-MA ratio in the matrix was varied, keeping the clay concentration constant at 5 wt %. The formulations for this set are presented in Table II.

Set 2

This set of formulations was prepared to examine the ability of the proposed parameters to consistently quantify samples with similar states of dispersion. Four samples were prepared from a single formulation by mixing for different times in the extruder. From prior experience, a 2 min processing time is known to be sufficient for obtaining maximum possible dispersion for the materials under consideration.[30] Therefore, providing longer processing times is expected to create samples with a similar degree of dispersion. The formulations for this set are presented in Table III.

Set 3

This set of formulations was prepared to examine the ability of the proposed parameters to capture independent aspects of dispersion. Four samples with different clay wt % but the same matrix composition were prepared. Increasing the clay wt % is expected to decrease the inter-particle distance, whereas the effect of the clay wt % on the exfoliation number is unknown. To provide maximum resolution for the exfoliation number, the formulations were compounded using PP-*g*-MA as the base resin to ensure the maximum degree of exfoliation. The formulations for this set are presented in Table IV.

Set 4

This set of formulations was prepared to examine the ability of the proposed parameters to resolve changes in dispersion due to simultaneous changes in more than one compositional parameter. The set contains two subsets each containing three samples with different clay wt %. The samples in one of the subsets had PP-*g*-MA/clay ratio of 0.5/1.0 and the other 1.0/1.0. The subset with PP-*g*-MA/clay ratio 0.5/1.0 was prepared by combining the masterbatch with PP homopolymer, impact modifiers, and elastomers. The subset with PP-*g*-MA/clay ratio 1.0/1.0 was prepared by adding additional PP-*g*-MA to the above formulation. The formulations of this set are presented in Table V.

Sample preparation

Among several demonstrated processing routes to prepare polymer–clay nanocomposites melt

TABLE II
Set 1: Formulations with Varying PP/PP-*g*-MA Ratio at Constant Clay wt %

Clay wt %	5	5	5	5	5
Sample name	Set 1–1	Set 1–2	Set 1–3	Set 1–4	Set 1–5
PH020	1.0	5.0	20.0	50.0	95.0
PP-*g*-MA	94.0	90.0	75.0	45.0	0.0
Cloisite 20A	5.0	5.0	5.0	5.0	5.0
FS 210 FF	0.2	0.2	0.2	0.2	0.2
Total	100.2	100.2	100.2	100.2	100.2

TABLE III
Set 2: Formulations with Varying Processing Time

Clay wt %	6	6	6	6
PP-*g*-MA/Clay	1.0/1.0	1.0/1.0	1.0/1.0	1.0/1.0
Processing time	2 min	5 min	10 min	15 min
Sample name	Set 2–1	Set 2–2	Set 2–3	Set 2–4
HA1152	17.6	17.6	17.6	17.6
KC130	17.6	17.6	17.6	17.6
CA138A	17.6	17.6	17.6	17.6
CA207A	17.6	17.6	17.6	17.6
Engage 8150	8.8	8.8	8.8	8.8
Masterbatch 70	8.6	8.6	8.6	8.6
PP-*g*-MA	3.4	3.4	3.4	3.4
PXH00A	8.8	8.8	8.8	8.8
FS 210 FF	0.2	0.2	0.2	0.2
Total	100.2	100.2	100.2	100.2

processing was chosen for this study because of its prevalence in the automotive and other compounding industries. Samples were prepared using a DSM Midi 2000 15 cm^3 micro-extruder and DSM injection molding machine. The extruder processing time was 2 min for Sets 1 and 3, 7 min for Set 4, and varying times for Set 2. Extrusions were run under an argon atmosphere. The screw rotation rate was 200 rpm, and the extrusion temperature was 180°C. Mold temperature was set at 50°C. The pack pressure was $\sim$ 90 psi (pneumatic), and pack time was $\sim$ 10 s. Samples were quickly removed from the mold and cooled to room temperature.

Transmission electron microscopy

TEM micrographs were obtained using a Philips 430t microscope operating at 300 kV and using thin sections (80 nm) prepared by cryo-microtomy using a Reichert Jung ultra-microtome at a temperature of −60°C. Micrographs at 21,000× magnification were produced to determine the extent of dispersion.

TABLE IV
Set 3: Formulations with Varying Clay wt % in PP-*g*-MA Matrix

Clay wt %	1	2	3	5
Sample name	Set 3–1	Set 3–2	Set 3–3	Set 3–4
PP-*g*-MA	99	98	97	95
Cloisite 20A	1	2	3	5
Total	100	100	100	100

DISPERSION QUANTIFICATION

There are two kinds of information in a 3D structure: (1) metric and (2) topological. The information about the metric properties is present, whereas that about the topological properties is not present in a 2D section of the 3D structure. On the one hand, a random heterogeneous microstructure, a surface, and a line in 3D would appear as an area, a line, and a point in a 2D section, respectively, and, therefore, it can be measured. It can be shown that there exist exact relationships between the volume fraction in 3D and area fraction in 2D, surface area per unit volume in 3D and perimeter of the corresponding traces per unit area in 2D, and length of lines per unit volume in 3D and the corresponding number of points per unit area in 2D without any assumption about the shape and the size distribution of the individual phases.[27–29] On the other hand, a point in 3D would not appear in a 2D section and, therefore, cannot be measured. Number density of particles in 3D cannot be measured from 2D sections without any assumption about the shape of the individual phases. Assuming that the clay particles are flat and convex in shape, the mean particle size in 3D can be determined. Further assuming that the clay particles are circular disks, the size-orientation distribution of the particles in 3D can be obtained. However, in the present work no assumption about the shape, size distribution, and the orientation distribution of the clay particles have been made, and two parameters, exfoliation number (ξ) and mean inter-particle

TABLE V
Set 4: Formulations with Varying Clay wt % at Two Different PP-*g*-MA/Clay Ratio

Clay wt %	3	3	6	6	9	9
PP-*g*-MA/Clay	0.5/1.0	1.0/1.0	0.5/1.0	1.0/1.0	0.5/1.0	1.0/1.0
Sample name	Set 4–1	Set 4–2	Set 4–3	Set 4–4	Set 4–5	Set 4–6
HA1152	47.8	46.9	45.6	43.9	43.5	40.9
CA138A	23.9	23.4	22.8	22.0	21.7	20.5
CA207A	23.9	23.4	22.8	22.0	21.7	20.5
Masterbatch 70	4.3	4.4	8.7	8.6	12.9	12.9
PP-*g*-MA	–	1.7	–	3.4	–	5.2
FS 210 FF	0.2	0.2	0.2	0.2	0.2	0.2
Total	100.1	100.0	100.1	100.1	100.0	100.2

distance (λ), have been developed[16] based on the metric properties of the 3D nanostructure to quantify the 3D extent of clay exfoliation and dispersion in polymer–clay nanocomposites. The exfoliation number is a measure of the percentage of the clay particles in the nanocomposite that are in direct contact with the polymer matrix. It is, therefore, represented as the ratio of polymer–clay interfacial surface area to total clay surface area both per unit volume of the nanocomposite:[16]

$$\xi = \frac{100(S_V)_{\mathrm{P-C}}}{(S_V)_{\mathrm{Total}}}. \quad (1)$$

Here, $(S_V)_{\mathrm{P-C}}$ and $(S_V)_{\mathrm{Total}}$ are polymer–clay interfacial surface area per unit volume in 3D and total clay surface area per unit volume in 3D, respectively.

The mean inter-particle distance is the mean of all straight line distances between arbitrary points on the surfaces of clay particles in 3D:[16]

$$\lambda = \frac{4(1 - V_V)}{(S_V)_{\mathrm{P-C}}}. \quad (2)$$

Here, V_V is the volume fraction of the clay particles.

Polymer–clay interfacial surface area per unit volume in 3D, $(S_V)_{\mathrm{P-C}}$, can be determined by measuring the perimeter of the traces of the clay particles per unit area, $(L_A)_{\mathrm{P-C}}$, from the 2D TEM micrograph:[29]

$$(S_V)_{\mathrm{P-C}} = \frac{4(L_A)_{\mathrm{P-C}}}{\pi}. \quad (3)$$

The total clay surface area per unit volume in 3D, $(S_V)_{\mathrm{Total}}$, can be determined by dividing the clay volume fraction by the thickness of a single clay platelet, t_{Platelet}:[16]

$$(S_V)_{\mathrm{Total}} = \frac{2V_V}{t_{\mathrm{Platelet}}}. \quad (4)$$

The factor 2 in the above equation accounts for the surface area associated with the two sides of the clay platelet.

Volume fraction of the clay particles, V_V, can be estimated by use of the Cavalieri principle by measuring the area fraction of the traces of the clay particles, A_A, from 2D TEM micrographs:[29]

$$V_V = A_A. \quad (5)$$

The 2D stereological parameters perimeter per unit area, $(L_A)_{\mathrm{P-C}}$, and area fraction, A_A, of the traces of the clay particles are measured from the TEM micrographs of the nanocomposite samples by quantitative image analysis. The image analysis procedure and a critical evaluation of the challenges involved are presented below.

IMAGE ANALYSIS

Image analysis of the TEM micrographs of polymer–clay nanocomposite samples for measurement of 2D stereological parameters involves two steps. First, binary images with clay particles and a polymer matrix as two distinct phases are created from their corresponding grayscale TEM micrographs. Second, 2D stereological parameters such as area fraction and perimeter of the traces of clay particles are measured from the binary micrographs. For both steps, commercial image analysis software Image-Pro Plus 5.0 was used. Details of these two steps are presented below.

Grayscale to binary conversion

Automatic segmentation of grayscale images containing a discontinuous second phase to binary images by image analysis software typically works on the principal of segmenting the image into two parts based on a threshold pixel intensity. All pixels with a higher intensity than the threshold value are designated as the first phase, and the rest of the pixels are designed as the second phase. Such binary segmentation of TEM micrographs of polymer–clay nanocomposites most often is not possible due to poor grayscale resolution of the micrographs, which appears to be due to thickness variation of the TEM samples.[31] Further complications in analysis can arise from difference in thicknesses between microtomed samples and the resulting variation in resolution of the corresponding TEM micrographs. Segmentation of the grayscale images to binary images is a prerequisite for any TEM-based quantitative analysis. Efficient software-based auto-segmentation requires sufficient spatial and grayscale resolution in the grayscale image and a sophisticated image segmentation algorithm capable of distinguishing clay particles from background noise. In absence of either, the segmentation process can become laborious requiring extensive manual tracing and correction. The micrographs used in this specific study had reasonable spatial and grayscale resolution; the commercial image analysis software used was only able to partially capture the clay particles. Therefore, automated software-based image segmentation followed by manual particle tracing/correction was utilized to prepare segmented binary micrographs. Figure 1(A,B) show a zoomed view of a grayscale micrograph and the corresponding binary TEM image of a typical polymer–clay nanocomposite sample used in this study. Once the binary image was

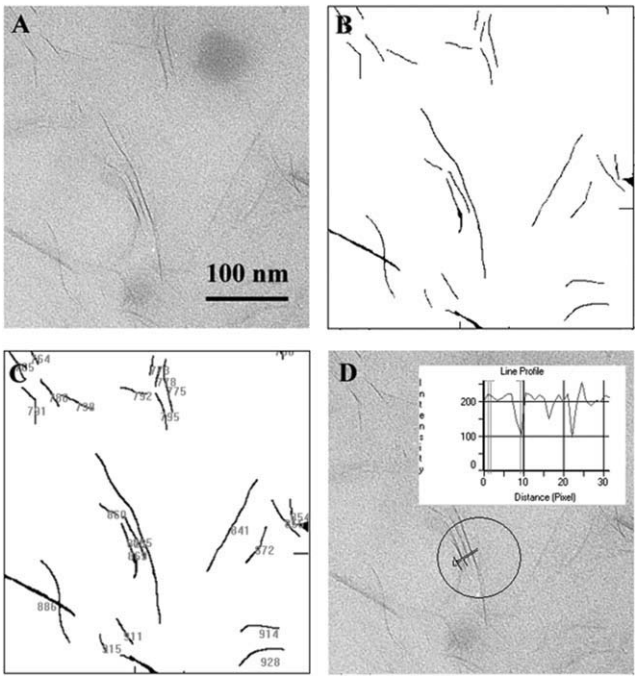

Figure 1 Conversion of TEM micrograph from grayscale to binary and subsequent measurement of 2D stereological parameters: (A) a typical grayscale TEM micrograph, (B) corresponding binary image, (C) measurement of 2D stereological parameters by Image-Pro Plus, and (D) measurement of pixel intensity along a straight line across fully exfoliated particles. The micrographs shown are zoomed sections of 100 times larger micrographs on which the measurements were carried out.

prepared, both the grayscale micrograph and the binary image were simultaneously examined for unintentional omission/addition of particles. Further, pixel intensity measurements across a line profile [as shown in Fig. 1(D)] were used on both micrographs to ensure that the thicknesses of the individual particles are kept equal in both cases. In case there are differences in the thickness of individual particles between these two micrographs, dilation/erosion of the discontinuous phase of the binary micrograph was used to match the particle thicknesses. However, it should be noted that dilation/erosion should be used with caution because these operations can cause unintentional joining/braking of particles. The final binary micrographs thus prepared were used for measuring 2D stereological parameters.

Measurement of 2D stereological parameters

The 2D stereological parameters were measured from the segmented binary TEM micrographs using Image-Pro Plus. The micrographs shown in Figure 1 are only representative zoomed sections presented for illustrative purpose. The measurements were carried out on micrographs 100 times larger. Figure 1(C) shows a visual representation of the measurement process by Image-Pro Plus. The total number of particles, the size of the micrograph (area, length $\times$ width, pixels), and the perimeter (pixels), area (pixels), and length (pixels) of each individual particle were measured. All particles with area less than 20 pixels were considered as noise and were excluded from further calculations. Thicknesses of individual particles were calculated by dividing the area by the length. The area fraction of the traces of the particles, A_A, was calculated by adding the areas of all the particles and dividing it by the area of the micrograph. Similarly, the perimeter of the traces of the clay particles per unit area, $(L_A)_{P-C}$, and the number of particles per unit area, N_A, were calculated by dividing the sum of the perimeters of all particles and the number of particles by the area of the micrograph, respectively. The aforementioned parameters with units in terms of pixels were converted into SI units using the scale bar of the micrograph. However, as converting particle thickness information from pixels to SI units, one extra caution was exercised. Because of scattering of the electrons, a single exfoliated MMT platelet with theoretical thickness of 0.94 nm[1] may not always appear so in the TEM micrographs. One such example is shown in Figure 1(D). For this specific micrograph, 1 pixel is equivalent to 1 nm. It has been shown with help of a line intensity profile measured perpendicularly across three fully exfoliated platelets that, in this specific case, the MMT platelet thickness appears as $\sim$ 2.5 nm. In such cases, this modified value for platelet thickness was used in eq. (4). This approach, though sound for correcting apparent thickness measurements of completely exfoliated and intercalated particles, may become tricky for unexfoliated, virgin particles, wherein there is not a direct way of verifying the apparent thickness of single platelets within the agglomerates. In such cases, XRD analysis results for the sample should be used judiciously in conjunction with the TEM micrographs for correcting the thickness information. In the results and discussion section that follow, apparent thickness correction is not made to the mean particle thickness reported. This is because, in this section, mean particle length and thickness are reported only to compare their effectiveness in capturing effects of compositional/processing parameters on the nanocomposite microstructure to that by the 3D stereological parameters, exfoliation number and inter-particle distance.

The stereological and traditional 2D and 3D parameters measured and evaluated in this article are influenced by grayscale to binary segmentation and statistical sampling errors. Because the main objective of this article is development and analysis of image segmentation-based 3D dispersion quantifying parameters, the segmentation errors are of more

relevance to this study. The statistical sampling error is well known and inherent to all TEM-based quantitative analysis/parameters. Therefore, the errors associated with the segmentation process and its effect on various parameters is evaluated in detail, whereas statistical sampling errors are only briefly discussed at the later part of the article.

The segmentation process can have a perceptible effect on the values of the 2D and 3D stereological parameters measured from the micrographs. It can be seen in from the line intensity profile measured perpendicularly across fully exfoliated platelets in Figure 1(D) that the intensity changes from its highest value to its lowest value gradually over several pixels (1 pixel = 1 nm in this specific case). Therefore, the threshold intensity used to segment the phases would have a major effect on quadratic parameters such as the area of the clay phase, but a minor effect on linear parameters such as the perimeter of the clay phase. Because all particles with less than 20 pixels area are excluded from analysis, change in segmentation intensity threshold would also have a minor effect on the number of particles. The standard deviation of error due to overestimation or underestimation of a linear feature such as length and thickness by one pixel during the segmentation process is included for the measured/calculated 2D/3D stereological parameters.

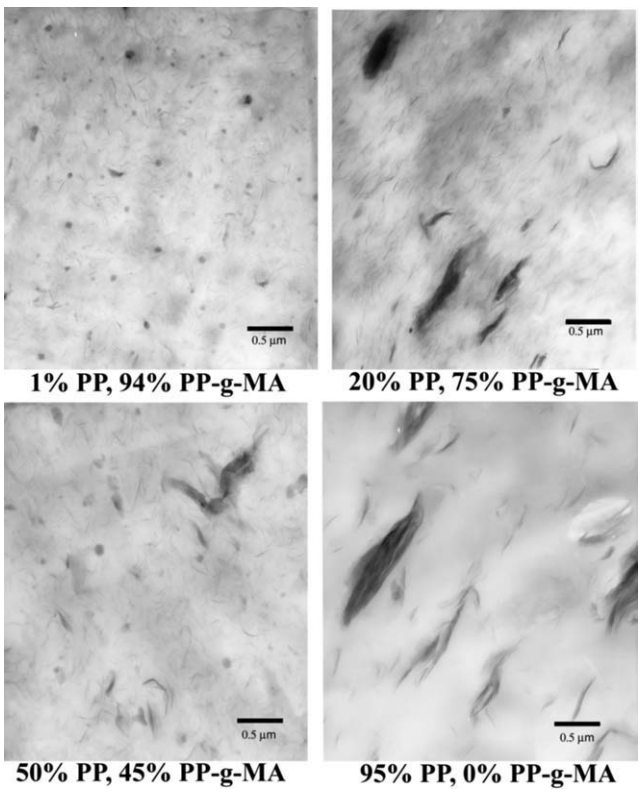

Figure 2 TEM micrographs of the samples in Set 1: formulations with varying PP to PP-*g*-MA ratio at constant clay wt %. The length bar presented in each micrograph is 0.5 μm long.

RESULTS AND DISCUSSION

In this section, the ability of the proposed 3D parameters, exfoliation number and inter-particle distance, to capture different aspects of dispersion in samples with a wide range in exfoliation is investigated. The quantification of the dispersion by exfoliation number and inter-particle distance is further critically compared against the standard 2D dispersion quantifying parameters such as mean length, thickness, and aspect ratio of the particles. As explained earlier, four sets of PP/PP-*g*-MA/Clay nanocomposite samples were prepared for examining the different aspects of dispersion quantification.

The samples in Set 1 were prepared to examine the ability of the exfoliation number and inter-particle distance parameters to capture dispersion in samples with a broad range of exfoliation. Figure 2 shows the grayscale TEM micrographs of the samples in this set. Figure 3 compares the exfoliation number and the inter-particle distance to the mean particle length, thickness, aspect ratio, and number of particles per unit area. All the parameters were measured from the binary TEM images corresponding to the grayscale micrographs shown in Figure 2. From visual inspection of the micrographs in Figure 2, it is evident that decreasing the PP to PP-*g*-MA ratio in the matrix at a constant clay wt % increases the extent of exfoliation. This is evidenced by the decrease in number of big agglomerates and the increase in the number of fully exfoliated single platelets. Increasing the ratio of the compatibilizer PP-*g*-MA in the matrix enhances matrix-clay compatibility by improving matrix polarity leading to better interaction and transfer of stress during extrusion, and thereby improving the extent of exfoliation. The qualitative visual assessment fails to gage the magnitude of improvement in the extent of exfoliation achieved by decreasing the PP to PP-*g*-MA ratio in the matrix, which can be quantitatively estimated by the proposed 3D stereological parameters. Figure 3 shows that decreasing PP to PP-*g*-MA ratio increases the exfoliation number and decreases the inter-particle distance. At a constant clay wt %, inter-particle distance varies inversely with exfoliation number [eq. (2)]. As a consequence, a monotonically increasing trend of the exfoliation number with decreasing PP to PP-*g*-MA ratios creates a monotonically decreasing trend for the inter-particle distance, which falls from 600 nm to 180 nm as the extent of exfoliation rises from less than 10% to more than 90%. Successful quantification of dispersion in samples at both extremes of exfoliation by the exfoliation number and inter-particle distance parameters demonstrate their capability of capturing dispersion in samples over the entire possible range.

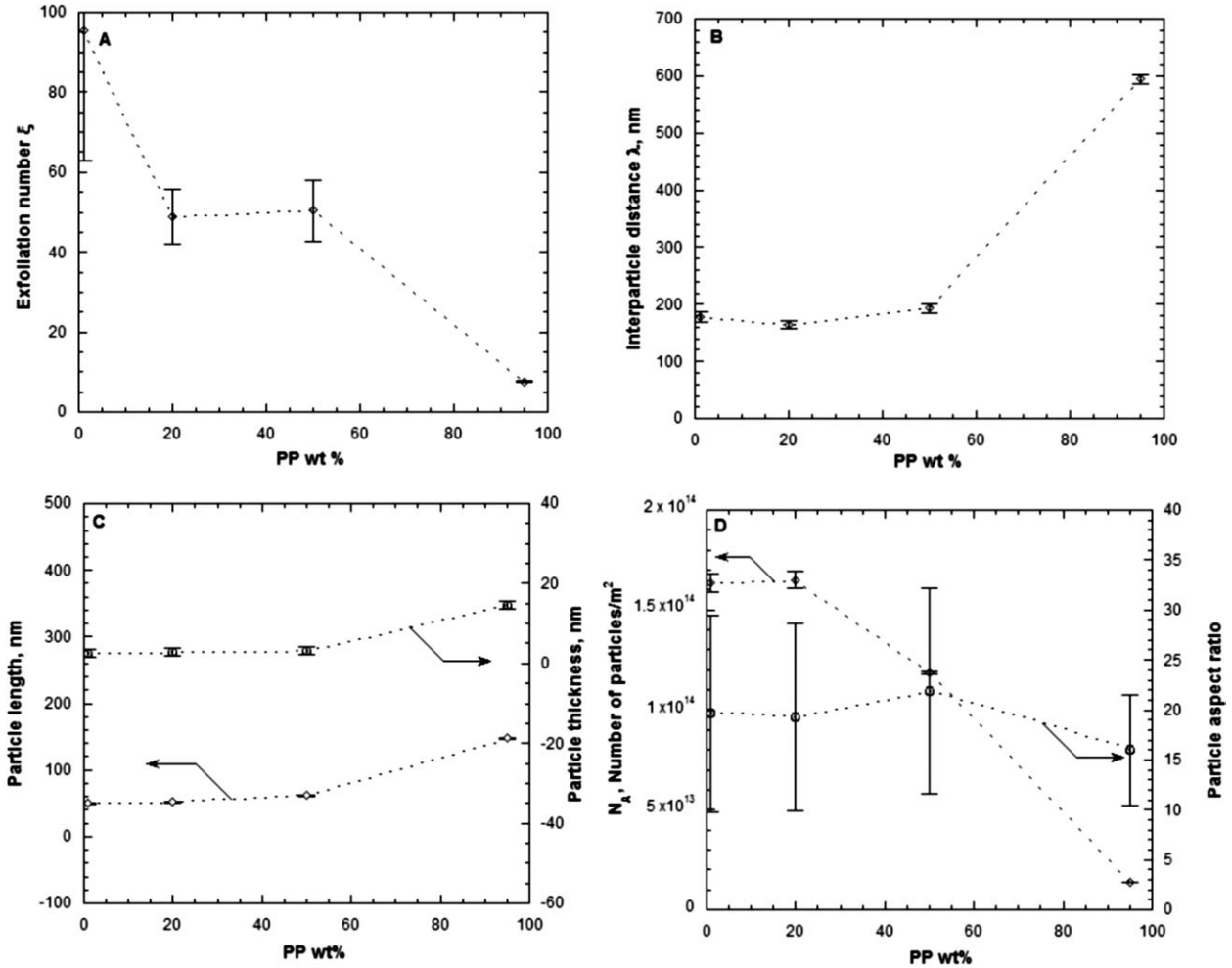

Figure 3 (A) Exfoliation number and (B) inter-particle distance compared with (C) mean length & thickness, and (D) aspect ratio & number of particles per unit area for the samples in Set 1. The error bars indicate standard deviation of the image segmentation and measurement procedure.

Table VI presents the 2D and 3D stereological parameters used to calculate the exfoliation number and inter-particle distance for the samples in Set 1. As a direct consequence of decreasing the PP to PP-*g*-MA ratio in the matrix, the total number of particle traces in 2D and polymer–clay interfacial area per unit volume in 3D both increase, indicating better exfoliation.* In contrast to the 3D stereological parameter, 2D parameters such as mean particle length and thickness decrease with decreasing PP to PP-*g*-MA ratio, i.e., increasing exfoliation (Fig. 3). This is presumably because, at a low degree of exfoliation, a large number of clay platelets stick together to form agglomerates. All the platelets in an agglomerate need not necessarily stack in uniform registry to each other, and, therefore, the agglomerate appears as a particle with large length and thickness. Occurrences of large agglomerated particles decrease with an increase in exfoliation, and hence, the mean particle length and thickness falls. On the one hand, this trend of the exfoliation is partially evident from the mean aspect ratio values of these samples, which is expected to increase with an increase in exfoliation. On the other hand, the number of particle traces per unit area increases sharply with an increase in exfoliation. The 3D parameters, exfoliation number and inter-particle distance appear to quantify microstructural aspects of the entire possible range of exfoliation and dispersion with comparable resolution as

*It should be noted that the measured 2D particle area fraction, and consequently, the 3D total clay surface area per unit volume decrease with decreasing PP/PP-*g*-MA ratio, whereas, at constant clay wt %, they are expected to stay constant. This demonstrates an important aspect of interpreting dispersion from TEM micrographs. In samples with a lower degree of exfoliation, particle area fraction can be overestimated in cases where the TEM micrographs have poor spatial resolution within unexfoliated agglomerates. However, at low-clay volume fraction (typical to polymer–clay nanocomposites), this overestimation in area fraction does not have any effect on the estimation of inter-particle distance but can cause slight underestimation of exfoliation number.

TABLE VI
Measured 2D and 3D Stereological Parameters for Set 1: Formulations with Varying PP/PP-*g*-MA Ratio at Constant Clay wt %

PP/PP-*g*-MA/Clay wt %	1/94/5	20/75/5	50/45/5	95/0/5
Number of particles	2396 ± 69	2316 ± 58	1658 ± 10	199 ± 2
Measured particle area fraction	0.025 ± 0.0086	0.052 ± 0.0091	0.043 ± 0.0077	0.089 ± 0.0022
Polymer–clay surface area per unit volume (nm^{-1})	0.0219 ± 0.00083	0.023 ± 0.00084	0.0198 ± 0.00060	0.006 ± 0.00007
Total clay surface area per unit volume (nm^{-1})	0.0229 ± 0.0078	0.047 ± 0.0082	0.039 ± 0.0069	0.081 ± 0.0020

The standard deviation of the image segmentation and measurement procedure is indicated.

the standard 2D quantifiers mean particle length, thickness, aspect ratio, and number of particle traces per unit area.

The samples in Set 2 were prepared with similar states of dispersion to examine the consistency of the exfoliation number and inter-particle distance parameters. Figure 4 shows the grayscale TEM micrographs of the samples in this set. Figure 5 compares the exfoliation number and the inter-particle distance to the mean length, thickness, aspect ratio, and number of particles per unit area. From visual inspection of the micrographs in Figure 4, samples of Set 2 qualitatively appear to be at similar states of dispersion. The exfoliation number and the inter-particle distance measurements shown in Figure 5 quantitatively confirm that the difference in the extent of dispersion among the samples is less than ±10%. This observation clearly demonstrates the consistency of the exfoliation number and inter-particle distance parameters in quantifying dispersion.

Table VII presents the 2D and 3D stereological parameters used to calculate the exfoliation number and the inter-particle distance for the samples in Set 2. The 3D parameters (polymer–clay interfacial area per unit volume and total clay surface area per unit volume), and the 2D parameters (mean particle length, thickness, aspect ratio, and number of particles per unit area as presented in Fig. 5) all consistently quantify similar states of dispersion among the samples. Therefore, when the samples do not have much difference in the extent of dispersion, then the exfoliation number and the inter-particle distance along with other 3D quantifiers and standard 2D quantifiers all consistently quantify a similar extent of dispersion.

The samples in Set 3 were prepared to examine whether the exfoliation number and inter-particle distance parameters capture independent aspects of dispersion. Figure 6 shows TEM micrographs of the samples of this set, each containing a different clay concentration. Figure 7 compares the exfoliation number and the inter-particle distance to the mean length, thickness, aspect ratio, and number of particles per unit area. The number of particles observed in the TEM micrographs expectedly increase with an increase in the clay wt %. However, visual observation of the micrographs does not reveal any information about the extent of exfoliation in these samples. Figure 7 shows that the exfoliation number does not change with increases in clay wt % indicating that the clay wt % does not have any effect on the extent of exfoliation, at least in well-exfoliated samples at low-clay loading (<10 wt %) such as these. Inter-particle distance decreases with clay wt % as a direct consequence of increases in number of particles per unit volume. Different effects of the clay wt % on exfoliation number and inter-particle distance clearly show that these two parameters are independent, and measure different aspects of dispersion.

Table VIII presents the 2D and 3D stereological parameters used to calculate the exfoliation number

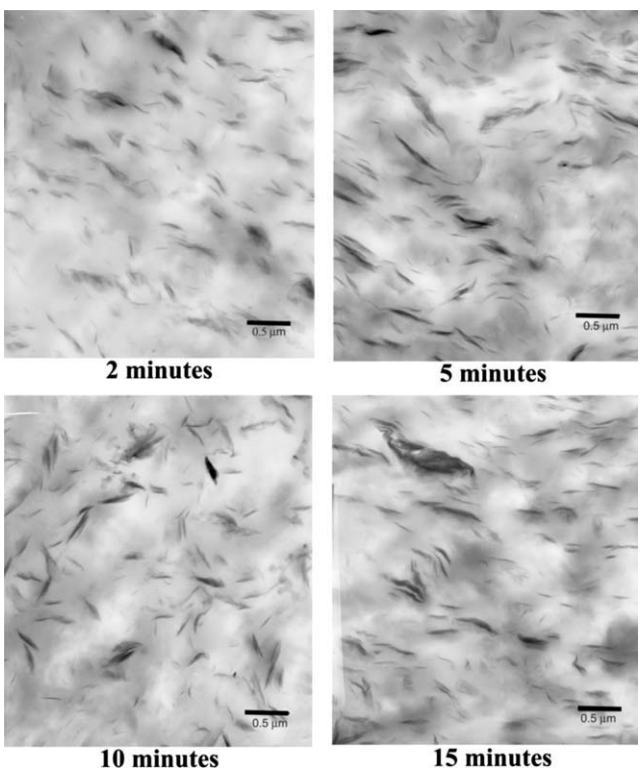

Figure 4 TEM micrographs of the samples in Set 2: formulations with varying processing time. The length bar presented in each micrograph is 0.5 µm long.

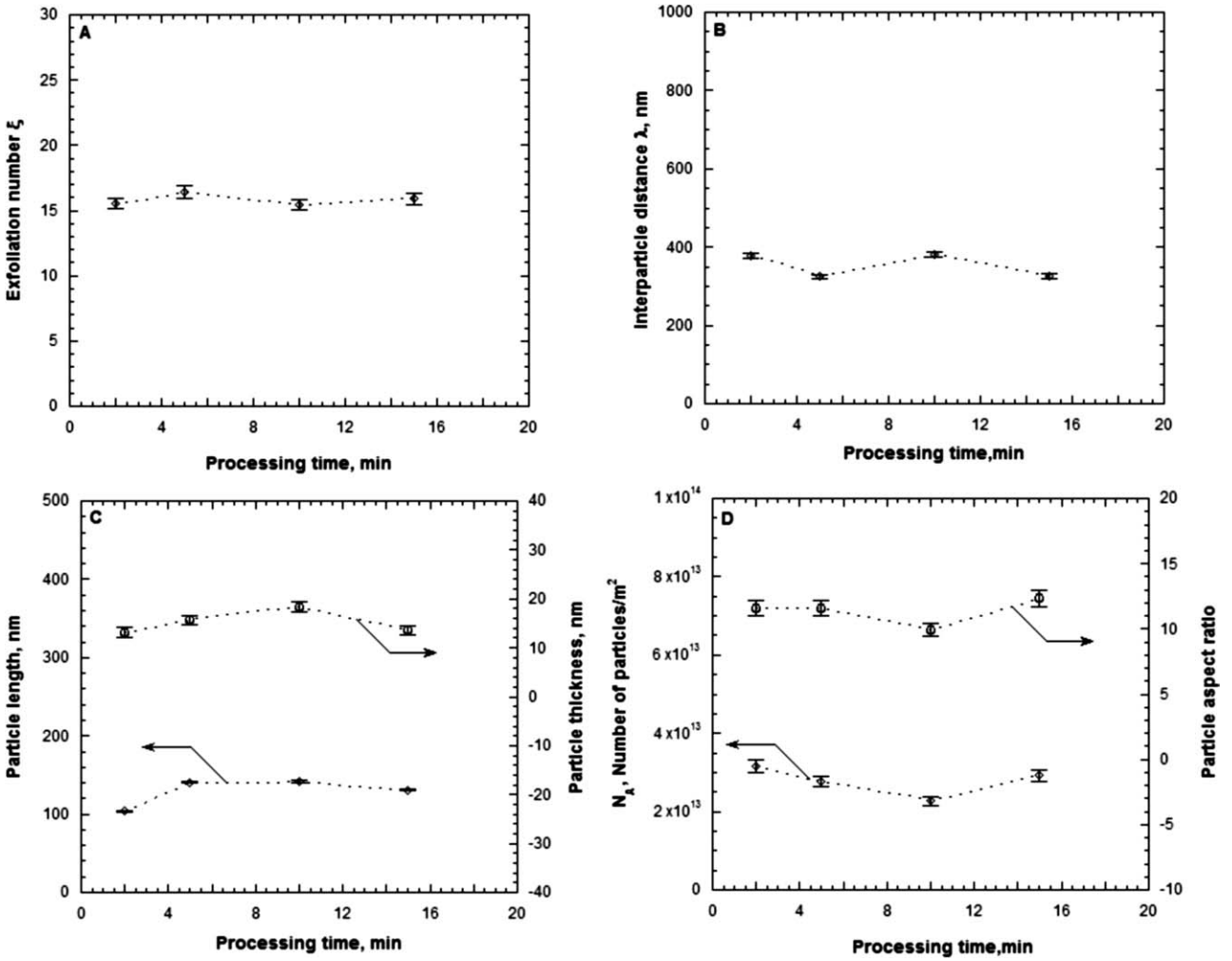

Figure 5 (A) Exfoliation number and (B) inter-particle distance compared with (C) mean length & thickness, and (D) aspect ratio & number of particles per unit area for the samples in Set 2. The error bars indicate standard deviation of the image segmentation and measurement procedure.

and the inter-particle distance for the samples in Set 3. Number of particles, area fraction of the particle traces, polymer–clay surface area per unit volume, and total clay surface area per unit volume are all found to increase as a direct consequence of an increase in the clay wt %. Increases in the clay wt % had no perceptible effect on mean particle thickness, whereas mean particle length and aspect ratio decreased only marginally. Typically, a decrease in the 2D aspect ratio is used as an indicator of the decrease in the extent of exfoliation; presumably a lower aspect ratio indicating several unexfoliated platelets stacked together. Therefore, from the aspect ratio data, one can infer that the degree of exfoliation decreases marginally with increases in the clay wt %. In contrast to that, exfoliation number measurements show that the extent of exfoliation does not change with increases in the clay wt %. For this set of samples, increases in the clay wt % is not expected to have any effect on the extent of exfoliation because at low-clay loadings, the nanocomposite remains dilute, hence particle–particle interaction and melt viscosity are low and cannot affect the shear field inside the extruder enough to change the extent of exfoliation. The fact that increasing the clay wt % has no significant effect on the extent of exfoliation of these samples is well captured by the 3D exfoliation number but is somewhat misinterpreted by the 2D aspect ratio measurement. The effect of the clay wt % on the spatial separation of clay particles is well captured by both the 3D inter-particle distance and the 2D number of particle traces per unit area.

The samples in Set 4 were prepared to examine whether the exfoliation number and inter-particle distance parameters are able to resolve changes in dispersion due to simultaneous changes in more than one compositional parameter. For this purpose, one subset of three samples with different clay wt % and a PP-*g*-MA to clay ratio of 0.5/1.0 was prepared.

TABLE VII
Measured 2D and 3D Stereological Parameters for Set 2: Formulations with Varying Processing Time

PP/PP-*g*-MA/Clay wt %	88/6/6	88/6/6	88/6/6	88/6/6
Processing time (min)	2	5	10	15
Number of particles	462 ± 3	401 ± 0	332 ± 0	425 ± 0
Measured particle area fraction	0.093 ± 0.0037	0.10 ± 0.0043	0.093 ± 0.0036	0.10 ± 0.0042
Polymer–clay surface area per unit volume (nm^{-1})	0.0096 ± 0.00016	0.011 ± 0.00014	0.0095 ± 0.00012	0.011 ± 0.00015
Total clay surface area per unit volume (nm^{-1})	0.062 ± 0.0025	0.067 ± 0.0029	0.062 ± 0.0024	0.069 ± 0.0028

The standard deviation of the image segmentation and measurement procedure is indicated.

A second subset with the exact same composition, except for a higher PP-*g*-MA to clay ratio of 1.0/1.0, was also prepared. Figure 8 shows the grayscale TEM micrographs of the samples in both subsets. Figure 9 compares the exfoliation number and the inter-particle distance to mean length, thickness, aspect ratio, and number of particles per unit area. Visual inspection of the micrographs qualitatively show that, at any constant clay wt %, a higher PP-*g*-MA to clay ratio produces samples with better exfoliation as evidenced by a decrease in the stack width and an increase in the number of particles. However, visual inspection of the samples with a constant PP-*g*-MA to clay ratio with different clay wt % does not reveal information about their state of exfoliation. Figure 9 shows that increasing the clay wt % at a constant PP-*g*-MA to clay ratio have little effect on the exfoliation number but causes the inter-particle distance to fall sharply. For the samples with same clay wt %, when the PP-*g*-MA to clay ratio is doubled, the exfoliation number shows a sharp $\sim$ 80% rise and the inter-particle distance shows a sharp $\sim$ 60% fall while preserving the trend with respect to the clay wt %. Distinctly separate clay wt % versus exfoliation number/inter-particle graphs for different PP-*g*-MA/clay ratios clearly demonstrate the ability of the exfoliation number and inter-particle distance parameters to resolve effects of simultaneous changes in more than one compositional parameter.

Table IX presents the 2D and 3D stereological parameters used to calculate the exfoliation number and the inter-particle distance for the samples in Set 4. For both subsets with constant PP-*g*-MA to clay ratios, the number of particles, the area fraction of the particle traces, the polymer–clay surface area per unit volume, and the total clay surface area per unit volume are all found to increase as a direct consequence of an increase in clay wt %. Across the subsets, an increase in the PP-*g*-MA to clay ratio at a constant clay wt % causes the number of particles and the polymer–clay surface area per unit volume to increase sharply, indicating better exfoliation, whereas the area fraction of particle traces and the total clay surface area per unit volume expectedly remain constant. For both subsets with constant PP-*g*-MA to clay ratio, an increase in the clay wt % marginally decreases the mean particle thickness and length, whereas the aspect ratio remains constant and the number of particle traces per unit area increases sharply. Across the subsets, increasing the PP-*g*-MA to clay ratio at a constant clay wt % causes the mean particle thickness, the length, and aspect ratio (unexpected) all to decrease marginally and the number of particles traces per unit area to increase sharply. It is evident from these observations that the 3D parameters, exfoliation number and inter-particle distance, are comparable with the standard 2D quantifiers in quantifying the microstructural effects of simultaneous changes in more than one compositional parameter.

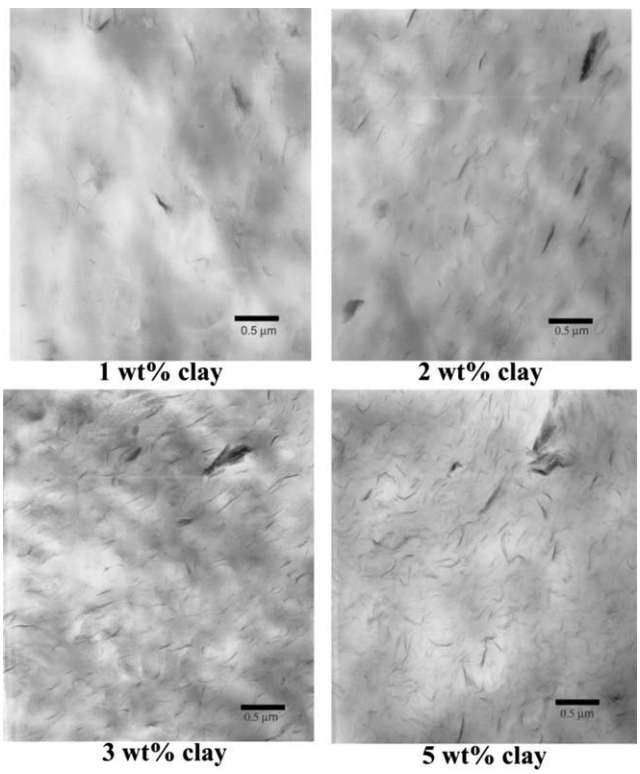

Figure 6 TEM micrographs of the samples in Set 3: formulations with varying clay wt %. The length bar presented in each micrograph is 0.5 μm long.

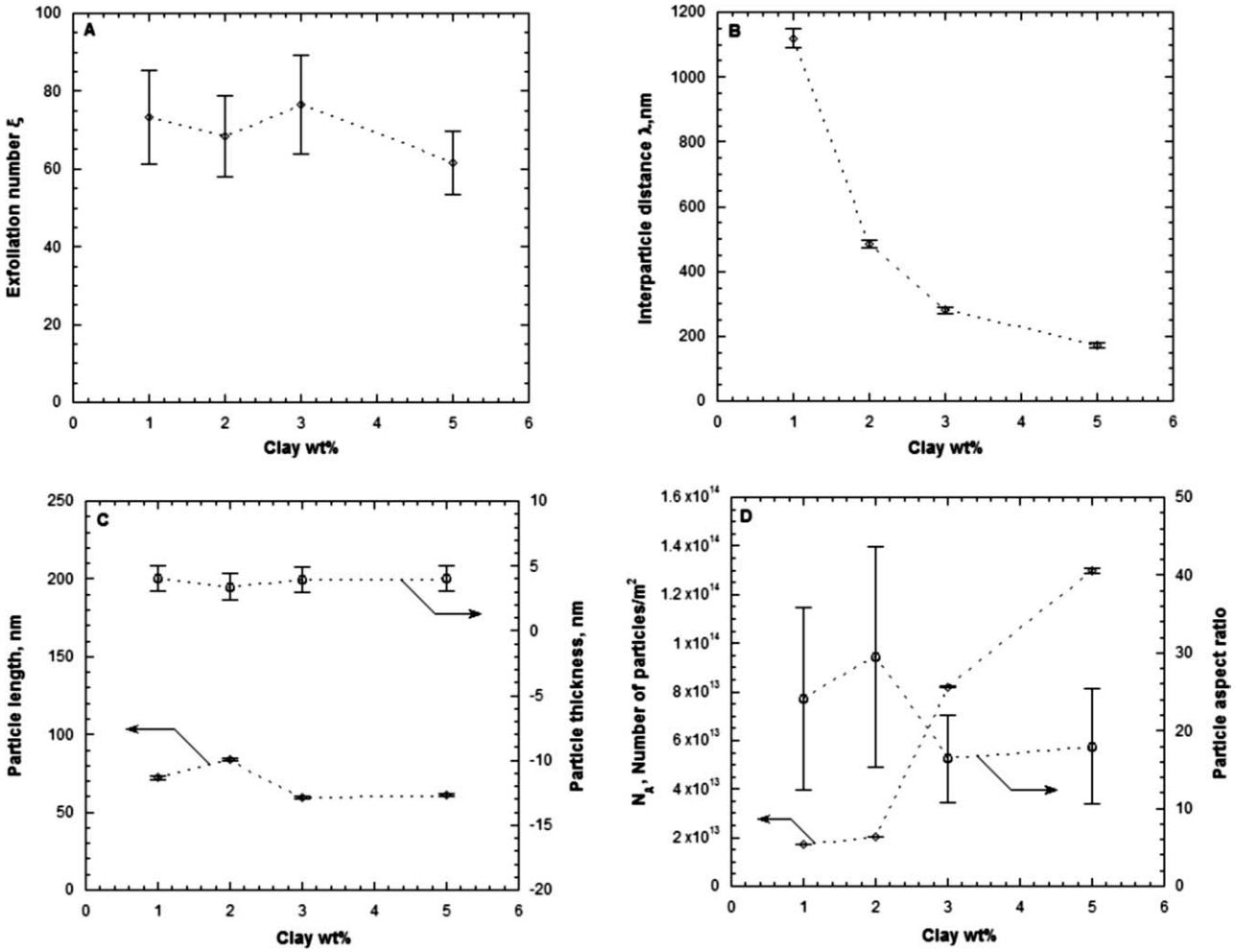

Figure 7 (A) Exfoliation number and (B) inter-particle distance compared with (C) mean length & thickness, and (D) aspect ratio & number of particles per unit area for the samples in Set 3. The error bars indicate standard deviation of the image segmentation and measurement procedure.

Stereological dispersion quantifying parameters measured from the binary TEM micrographs provide quantitative assessment of dispersion and nanostructure in polymer–clay nanocomposites rather than the qualitative assessment provided by visual inspection of the grayscale TEM micrographs. The proposed dispersion quantifying parameters, the exfoliation number and the inter-particle distance, by design are independent of the bias present in the standard 2D measurements such as mean length, thickness, and aspect ratio of the particles. The exfoliation number and the inter-particle distance provide a direct measurement of the extent of exfoliation and the spatial separation between clay particles rather than an indirect assessment of dispersion provided by mean particle aspect ratio, length and thickness distribution, and number of particle traces per unit area measurements. Moreover, the indirect assessment of the extent of exfoliation provided by the particle aspect ratio measurement (higher aspect ratio indicating better exfoliation) is valid only when all the platelets in a stack are aligned in a parallel fashion, which is not the case in most of the agglomerates observed in

TABLE VIII
Measured 2D and 3D Stereological Parameters for Set 3: Formulations with Varying Clay wt %

PP/PP-*g*-MA/Clay wt %	0/99/1	0/98/2	0/97/3	0/95/5
Number of particles	245 ± 0	481 ± 0	1188 ± 6	1859 ± 18
Measured particle area fraction	0.0073 ± 0.0013	0.018 ± 0.0030	0.027 ± 0.0052	0.054 ± 0.0085
Polymer–clay surface area per unit volume (nm^{-1})	0.0035 ± 0.00009	0.0081 ± 0.00018	0.014 ± 0.00042	0.022 ± 0.00066
Total clay surface area per unit volume (nm^{-1})	0.0048 ± 0.0009	0.012 ± 0.0020	0.01 ± 0.0035	0.036 ± 0.0056

The standard deviation of the image segmentation and measurement procedure is indicated.

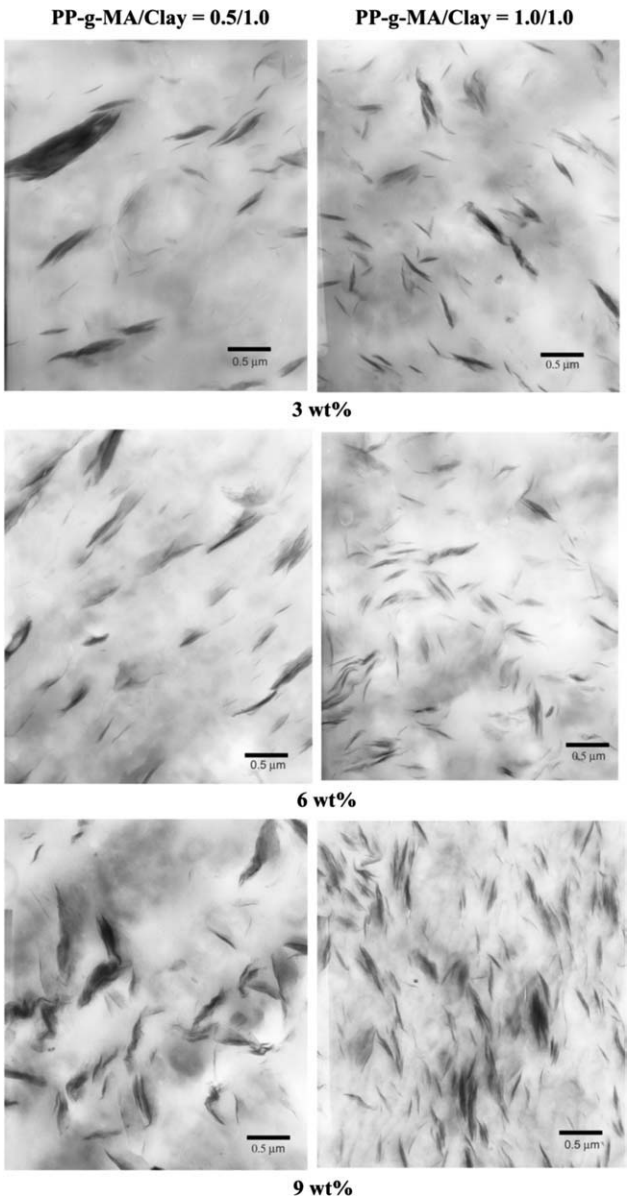

Figure 8 TEM micrographs of the samples in Set 4: formulations with varying clay wt % at PP-*g*-MA to Clay ratio 0.5/1.0 and 1.0/1.0. The length bar presented in each micrograph is 0.5 μm long (Reproduced with permission from Basu et al., Appl Phys Lett, 2007, 91, 053105, © American Institute of Physics).

less exfoliated samples. Inferring the extent of exfoliation from the mean values of the particle length, thickness, and aspect ratio introduces the additional error of using an arithmetic mean that assigns equal weight to all particles, whereas each particle should have a weight proportional to the number of platelets it contains. The exfoliation number and inter-particle distance parameters by definition are free of such errors.

The proposed parameters are able to successfully capture the same qualitative microstructural trends as captured by the traditional 2D parameters as being independent of the bias present in the 2D measurements. The resolution, range, and consistency of the proposed 3D parameters in terms of their ability to quantify the details of the nanostructure are comparable with the traditional 2D parameters. However, how well the proposed 3D parameters capture the effects of nanostructure/dispersion on the thermophysical properties of the nanocomposite compared with the traditional 2D parameters remains unknown, and further research is needed in this direction. Moreover, the proposed 3D parameters λ, ξ, and the traditional 2D parameters length, thickness, aspect ratio measure separate aspects of the nanostructure, and therefore, different parameters are expected to have different degrees of bearings on each thermophysical property. According to composite theory, the aspect ratio of the clay particles is the most important parameter for predicting the thermophysical properties of the nanocomposite. Deconvolution of the bias present in 2D measurement of aspect ratio involves deconvolution of the bias present in the 2D length and thickness measurements. The 3D length distribution can be deconvoluted from the measured 2D length distribution by assuming circular disk-shaped clay particles and assuming the existence of an axis of symmetry within the microstructure as per Gokhale.[32] The 3D thickness distribution deconvolution using a similar procedure remains more challenging due to additional difficulties of precise measurement of clay platelet thicknesses from the TEM micrographs.

The nanostructure quantifiers proposed in this work provide an analysis framework wherein the information present in the 2D micrographs can be quantitatively analyzed without the bias present in the 2D measurement. Although the exfoliation number and inter-particle distance parameters are shown to be versatile, independent, and able to capture different aspects of dispersion, their applicability in certain instances could be constrained due to the inadequate spatial and grayscale resolution in the TEM micrographs, the apparent increase in the thickness of the clay platelets due to scattering, and the human subjectivity included in the grayscale to binary segmentation and statistical sampling.[16] The effect of over and under estimation of the clay phase due to segmentation indicate that polymer–clay interfacial area per unit volume $(S_V)_{P-C}$ which is dependent on linear measure $(L_A)_{P-C}$ is not very sensitive to segmentation errors, whereas total clay surface area per unit volume $(S_V)_{Total}$ which is dependent on quadratic measure A_A is sensitive to segmentation errors. The exfoliation number $\xi \sim (L_A)_{P-C} t_{platelet}/A_A$ is inversely proportional to A_A and is sensitive to segmentation errors at low values of A_A, i.e., high values of ξ. The inter-particle distance

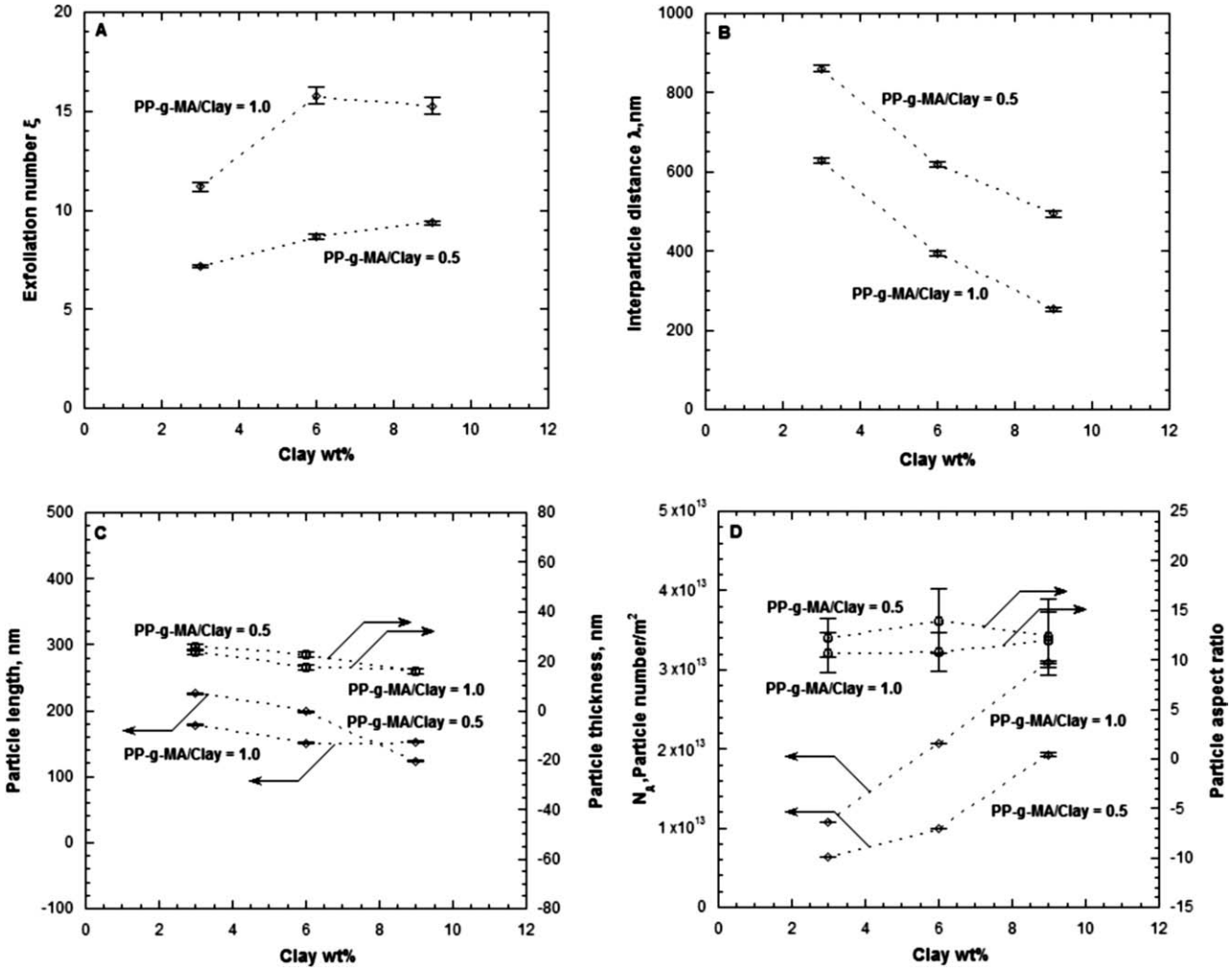

Figure 9 (A) Exfoliation number and (B) inter-particle distance compared with (C) mean length & thickness, and (D) aspect ratio & number of particles per unit area for the samples in Set 4. The error bars indicate standard deviation of the image segmentation and measurement procedure (Reproduced with permission from Basu et al., Appl Phys Lett, 2007, 91, 053105, © American Institute of Physics).

$\lambda \sim (1 - A_A)/(L_A)_{P-C} \sim 1/(L_C)_{P-C}$ (for $A_A \ll 1$) is not very sensitive to segmentation errors. The number of particles per unit area N_A is also not very sensitive to segmentation errors. Among the traditional 2D parameters, particle length is not very sensitive segmentation errors, whereas particle thickness is

TABLE IX
Measured 2D and 3D Stereological Parameters for Set 4: Formulations with Varying Clay wt % at PP-*g*-MA to Clay Ratio 0.5/1.0 and 1.0/1.0

PP/PP-*g*-MA/Clay wt %	95.5/1.5/3	94/3/3	91/3/6	88/6/6	86.5/4.5/9	82/9/9
Number of particles	91 ± 0	154 ± 0	147 ± 0	288 ± 0	277 ± 3	447 ± 3
Measured particle area fraction	0.089 ± 0.0016	0.079 ± 0.0022	0.101 ± 0.0022	0.088 ± 0.0035	0.115 ± 0.0027	0.134 ± 0.0052
Polymer–clay surface area per unit volume (nm^{-1})	0.0042 ± 0.00003	0.0059 ± 0.00005	0.0058 ± 0.00005	0.0093 ± 0.00011	0.0072 ± 0.00010	0.014 ± 0.00016
Total clay surface area per unit volume (nm^{-1})	0.059 ± 0.0011	0.052 ± 0.0014	0.067 ± 0.0015	0.059 ± 0.0023	0.076 ± 0.0018	0.089 ± 0.0035

The standard deviation of the image segmentation and measurement procedure is indicated.

only sensitive to segmentation errors at low values of thickness. Particle aspect ratio $A_r = l/t$ is sensitive to segmentation errors at low values of t, i.e., high values of A_r.

The statistical sampling error is inherent to any TEM-based quantitative analysis and is important since in TEM observations, only a small fraction of the total population is sampled. The extent of error due to sampling can be evaluated using the central limit theorem or the t-distribution statistics. For a given level of confidence, the t-distribution statistics can be used to calculate the amount of sampling (i.e., the size/number of TEM micrographs) required to have a desired interval of error. It should be noted that an increase in sampling N reduces the error, but the returns in terms of increased accuracy diminish because the error is proportional to the square root of N. These challenges can be reduced by using high-resolution TEM images at higher magnification and devising better image segmentation algorithms to enable auto-segmentation of the gray-scale TEM images.

The 3D dispersion quantifying parameters investigated and benchmarked in this paper enable researchers to establish processing/composition-nanostructure and nanostructure-property relationships in polymer–clay nanocomposites. Furthermore, these direct measurement-based dispersion quantifiers can be used to benchmark other indirect dispersion measurement techniques such as XRD, rheology, NMR, etc. It should be noted that the proposed 3D dispersion quantifying parameters are a different way to analyze the information present in 2D micrographs, which removes the bias associated with not sampling the true particle diameter. However, these parameters are still limited by the information available in the 2D micrograph and should not be considered as an alternative to direct 3D measurement such as electron tomography.

CONCLUSIONS

A stereology-based procedure for calculating the 3D dispersion quantifying parameters from the 2D TEM micrographs of polymer–clay nanocomposite samples has been proposed, and the challenges discussed. The stereology-based 3D dispersion quantification parameters, exfoliation number and inter-particle distance, were found to describe the extent of dispersion in samples over a wide range of exfoliation, to consistently quantify samples with a similar degree of dispersion, to capture mutually independent aspects of dispersion, and to resolve the effects of simultaneous changes in different compositional parameters on dispersion. Using a PP/PP-*g*-MA/clay system, it was found that at a constant clay wt %, increasing the percentage of the compatibilizer, PP-*g*-MA, in the matrix can increase the extent of exfoliation from less than 10% to more than 90%. At a constant matrix composition, increasing the clay wt %, however, had no effect on extent of exfoliation. Increases in the extent of exfoliation due to a change in the matrix composition and increases in particle density due to an increase in the clay wt % were both found to decrease the inter-particle distance.

Critical comparison of the 3D dispersion quantifying parameters, exfoliation number and inter-particle distance, against the standard 2D dispersion quantifying parameters such as mean length, thickness, and aspect ratio of particles revealed that in terms of the ability to quantify dispersion of the nanostructure, the sensitivity, resolution, and segmentation error, the proposed 3D parameters are comparable with the standard 2D parameters. Furthermore, the proposed 3D parameters, by design, are free from the bias present in the 2D parameters that produce erroneous mean values of the 3D quantities they represent. The proposed approach measures those 2D quantities from the segmented TEM micrographs which have exact stereological relationships with 3D microstructural attributes, and thereby eliminates the bias present in the traditional 2D measurements. Development of these versatile nanostructure quantification parameters enables researchers to establish processing structure–property relationships in nanocomposites, and thereby design better nanocomposites.

The authors thank Dr. Asim Tewari of ISL, GM R&D for invaluable discussions.

References

1. Pinnavaia, T. J.; Beall, G. W. Polymer-Clay Nanocomposites; Wiley: New York, 2000.
2. Vaia, R. A.; Giannelis, E. P. MRS Bull 2001, 26, 394.
3. Yang, Y.; Zhu, Z. K.; Yin, J.; Wang, X. Y.; Qi, Z. E. Polymer 1999, 40, 4407.
4. Liang, Z. M.; Yin, J.; Xu, H. J. Polymer 2003, 44, 1391.
5. Eckel, D. F.; Balogh, M. P.; Fasulo, P. D.; Rodgers, W. R. J Appl Polym Sci 2004, 93, 1110.
6. Marchant, D.; Jayaraman, K. Ind Eng Chem Res 2002, 41, 6402.
7. Dennis, H. R.; Hunter, D. L.; Chang, D.; Kim, S.; White, J. L.; Cho, J. W.; Paul, D. R. Polymer 2001, 42, 9513.
8. Nam, P. H.; Maiti, P.; Okamoto, M.; Kataka, T.; Hasegawa, N.; Usuki, A. Polymer 2001, 42, 9633.
9. Fornes, T. D.; Yoon, P. J.; Keskkula, H.; Paul, D. R. Polymer 2001, 42, 9929.
10. Lee, H. S.; Fasulo, P. D.; Rodgers, W. R.; Paul, D. R. Polymer 2005, 46, 11673.
11. Fornes, T. D.; Paul, D. R. Polymer 2003, 44, 4993.
12. Chavarria, F.; Paul, D. R. Polymer 2004, 45, 8501.
13. Vermogen, A.; Varlot, K. M.; Seguela, R.; Rumeau, J. D.; Boucard, S.; Prele, P. Macromolecules 2005, 38, 9661.

14. Ratinac, K. R.; Gilbert, R. G.; Ye, L.; Jones, A. S.; Ringer, S. P. Polymer 2006, 47, 6337.
15. Kim, D.; Lee, J. S.; Barry, G. M. F.; Mead, J. L. Microsc Res Tech 2007, 70, 539.
16. Basu, S. K.; Tewari, A.; Fasulo, P. D.; Rodgers, W. R. Appl Phys Lett 2007, 91, 053105.
17. Mollet, V. A.; Kamal, M. R. J Polym Eng 2006, 26, 757.
18. Wagener, R.; Reisinger, T. J. G. Polymer 2003, 44, 7513.
19. Zhao, J.; Morgan, A. B.; Harris, J. D. Polymer 2005, 46, 8641.
20. Durmus, A.; Kosgoz, A.; Macosko, C. W. Polymer 2007, 48, 4492.
21. Vermant, J.; Ceccia, S.; Dolgovskii, M. K.; Maffettone, P. L.; Macosko, C. W. J Rheol 2007, 51, 429.
22. Varlot, K.; Reynaud, E.; Kloppfer, M. H.; Vigier, G.; Varlet, J. J Polym Sci Part B: Polym Phys 2001, 39, 1360.
23. Ijdo, W. L.; Kemnetz, S.; Benderly, D. Polym Eng Sci 2006, 46, 1031.
24. Russo, G. M.; Simon, G. P.; Incarnato, L. Macromolecules 2006, 39, 3855.
25. Borse, N. K.; Kamal, M. R. Polym Eng Sci 2006, 46, 1094.
26. VanderHart, D. L.; Asano, A.; Gilman, J. W. Macromolecules 2001, 34, 3819.
27. Russ, J. C.; Dehoff, R. T. Practical Stereology; Springer: New York, 2000.
28. Mouton, P. R. Principles and Practices of Unbiased Stereology: An Introduction for Bioscientists; The Johns Hopkins University Press: Baltimore, 2002.
29. Underwood, E. E. Quantitative Stereology; Addison-Wesley: Massachusetts, 1970.
30. Rodgers, W. R.; Fasulo, P. D.; Ottaviani, R. A. First World Congress of Nanocomposites, Chicago, USA, June 25–27, 2001.
31. Williams, D. B.; Carter, B. C. Transmission Electron Microscopy; Plenum Press: New York, 1996.
32. Gokhale, A. M. Acta Mater 1996, 44, 475.